Progress In Electromagnetics Research B, Vol. 89, 177–194, 2020

Design of Ultra-High Gain Optical Micro-Amplifiers via Smart Nonlinear Wave Mixing

Özüm E. Aşırım[1, *] and Alim Yolalmaz[2]

Abstract—Optical amplification by nonlinear wave mixing offers wideband high-gain amplification that is desirable for a variety of applications. When the wave mixing process occurs in an interaction medium with sufficient length, the attained gain per excitation pulse is usually higher than that can be attained by lasers. Furthermore, the bandwidth of amplification via nonlinear wave mixing is much higher than the bandwidth allowed by laser transitions of laser gain media. However, optical amplification by nonlinear wave mixing offers negligible gain in the micrometer scale, due to a very limited length of the interaction medium. In micro-resonators, such a short interaction length does not offer sufficient small signal gain to compensate the round-trip loss. In this study, we present a Fletcher-Reeves algorithm-based nonlinear programming of the wave mixing process that tunes the frequencies of the excitation pulses of the source device in order to provide an ultra-high optical gain in the micro-scale via maximizing the electric energy density in a micro-resonator. Using this smart wave mixing approach, we obtained a micro-resonator gain of 4.7×10^7 for an input wave at 640 THz and a gain of 1.5×10^8 at 100 THz. The results of our mathematical formulation are compared with well-known experimental results, and a mean accuracy of 99% is observed. The study aims to show that optical amplifiers that are based on the principle of nonlinear wave mixing can be used in the micro-scale for wideband ultra-high gain operation.

1. INTRODUCTION

Optical parametric amplification (OPA) has been extensively studied and can be used for a variety of applications, such as photonic integrated circuits, high-speed optical communications, piezoelectric MEMS devices, and generation of intense laser beams. Optical parametric amplification is achieved via mixing a nonlinearity inducing high-intensity pump wave with an input wave of low intensity, during which the low-intensity input wave gets amplified by absorbing energy from the high-intensity pump wave. The rate and the amount of energy that can be transferred depends on the nonlinearity of the interaction medium. Hence, the gain of a parametric amplification process depends heavily on the length of the interaction medium. The required interaction medium length for high optical gain is usually on the order of centimeters.

There is an abundance of studies that have investigated the resonant nonlinear optical response of various materials via several experimental techniques [1–12]. These materials can be used for enhancing the optical gain that is attainable from a nonlinear wave mixing process. In fact, in the last two decades, there have been numerous studies that focused on enhancing the gain of optical parametric amplifiers. These studies [13–32] have mostly been experimental and have usually focused on the discovery, design, and employment of super-nonlinear media for optical gain enhancement. One experimental study in particular [21] has shown that a gain factor on the order of 10^5 is possible in the microscale via a

Received 22 October 2020, Accepted 7 December 2020, Scheduled 16 December 2020

* Corresponding author: Özüm Emre Aşırım (e176154@metu.edu.tr).

[1] Department of Electrical and Electronics Engineering, Middle East Technical University, Ankara 06800, Turkey. [2] Micro and Nanotechnology Department, Middle East Technical University, Ankara 06800, Turkey.

specially designed interaction medium. Another experimental study [18] has demonstrated a remarkable wideband gain in a 5 millimeter long, highly nonlinear interaction medium. However, to this date, there is no study that has made a direct attempt to maximize the gain factor using smart algorithms via computational approach. Smart algorithms can be employed in maximizing the gain factor of an input wave that is amplified via nonlinear wave mixing process as certain signal processing or machine learning algorithms. In this study, we will use a constrained nonlinear programming approach based on the Fletcher-Reeves algorithm that is both computationally cost efficient and has rapid convergence, by embedding it into the finite difference time domain (FDTD) discretization of the wave equation and the associated equations for the components of the polarization density corresponding to the resonance (emission) frequencies of an arbitrary interaction medium. The update equations of the algorithm will be solved in concurrence with the discretized equations.

Enhancing the optical gain of the nonlinear wave mixing process in the micro and nanoscale is a crucial scientific problem as its achievement can enable various new technologies based on micro and nanotechnology, such as novel ultra-wideband optical antennas, super-efficient harmonic generators, and small-scale optical ablation devices. It is also an important issue for creating more powerful macroscale high-power optical devices that can be used for many different purposes [34, 35, 37, 38].

In order to simplify the description of the whole procedure, the problem will be investigated in a plain Fabry-Perot type micro-resonator. We will start our analysis by reestablishing the mathematical background of optical amplification via nonlinear wave mixing. Then we will reintroduce and integrate the Fletcher-Reeves algorithm into the mathematical formulation of the nonlinear wave mixing process. The resonator parameters and the constraints imposed by the source device, based on the frequency tunability of the excitation pulses, will be the input parameters of the algorithm. The partial differential equations that model the parametric amplification will be discretized by the finite difference time domain (FDTD) method and will be solved iteratively along with the Fletcher-Reeves optimization process. The results will be presented through detailed computer simulations, and the employed computational model will be validated by the well-known experimental results of the sum-frequency generation process. The constructed computational model will be summarized in the conclusion.

2. METHODS

The Fabry-Perot micro-resonator that is modeled in this study has an optical isolator at the input port and a band-pass filter at the output port. The interaction medium (gain medium) is assumed to have multiple resonances. For an arbitrary interaction medium with N resonance (emission) frequencies, the mathematical description of the OPA process and the definitions of the involved parameters are explained as below:

$$\textit{Polarization decay rates of the medium of interaction}: \ \{\gamma_1, \gamma_2, \ldots, \gamma_N\}$$

$$\textit{Resonance (emission) frequencies of the medium of interaction}: \ \{f_1 f_2, \ldots, f_N\}$$

$$E_p: \textit{ Pump wave electric field intensity}, \quad P_p: \textit{ Total polarization density induced by the pump wave}$$

$$P_{p,l}: \textit{ Pump wave induced polarization density for the lth emission frequency of the medium}$$

$$E_{in}: \textit{ Input wave electric field intensity}, \quad P_{in}: \textit{ Total polarization density induced by the input wave}$$

$$P_{in,l}: \textit{ Input wave induced polarization density for the lth emission frequency of the medium}$$

$$\varepsilon_\infty: \textit{ Background permittivity of the medium}$$

$$\sigma: \textit{ Electrical conductivity of the medium}, \quad \mu_0: \textit{ Free space permeability}$$

$$Q_l: \textit{ Electron density corresponding to the lth resonance frequency}, \quad Q: \textit{ Total electron density}$$

$$\xi_l: \textit{ Resonance probabilities (oscillator strengths)}$$

The propagation of the pump wave (excluding the presence of the input wave) is described by Equations (1)–(2) [33, 34]. Equation (1) represents the electric field wave equation of the pump wave, and Equation (2) represents the associated polarization density components induced for each resonance frequency. Note that each resonance frequency is associated with a different polarization decay rate,

electron density, and polarization density. Therefore, the total polarization density in Equation (1) is the sum of all polarization densities indicated in Equation (2) ($P_p = P_{p,1} + P_{p,2} + \ldots + P_{p,N}$)

$$\nabla^2 (E_p) - \mu_0 \varepsilon_\infty \frac{\partial^2 (E_p)}{\partial t^2} = \mu_0 \sigma \frac{\partial (E_p)}{\partial t} + \mu_0 \frac{d^2 P_p}{\partial t^2} \tag{1}$$

$$\frac{d^2 P_{p,l}}{dt^2} + \gamma_l \frac{dP_{p,l}}{dt} + \omega_l^2 P_{p,l} - \frac{\omega_l^2 P_{p,l}^2}{Q_l e d} + \frac{\omega_l^2 P_{p,l}^3}{Q_l^2 e^2 d^2} = \frac{Q_l e^2 E_p}{m} \tag{2}$$

Quantum mechanics dictates that the sum of all resonance probabilities is equal to 1 [33–35]. Therefore, for a given electromagnetic wave in the medium of propagation, the relation between the resonance probabilities and the associated polarization density components at each resonance is summarized by the following equations

$$\sum_{l=1}^{N} \xi_l = 1, \tag{3}$$

$$P = \sum_{l=1}^{N} P_l = \sum_{l=1}^{N} Q_l p_l = Q \sum_{l=1}^{N} \xi_l p_l \tag{4}$$

where p_l is the induced electric dipole moment contributed by the lth resonance frequency of the medium.

When the low-intensity input wave and high-intensity pump wave are present in the same interaction medium, the total wave and associated polarization densities can be expressed by the following equations

$$\nabla^2 (E_p + E_{in}) - \mu_0 \varepsilon_\infty \frac{\partial^2 (E_p + E_{in})}{\partial t^2} = \mu_0 \sigma \frac{\partial (E_p + E_{in})}{\partial t} + \mu_0 \frac{d^2 (P_p + P_{in})}{\partial t^2} \tag{5}$$

$$\frac{d^2 (P_{p,l} + P_{in,l})}{dt^2} + \gamma_l \frac{d(P_{p,l} + P_{in,l})}{dt} + \omega_l^2 (P_{p,l} + P_{in,l}) - \frac{\omega_l^2 (P_{p,l} + P_{in,l})^2}{Q_l e d} + \frac{\omega_l^2 (P_{p,l} + P_{in,l})^3}{Q_l^2 e^2 d^2}$$

$$= \frac{Q_l e^2 (E_p + E_{in})}{m} \tag{6}$$

$$P_p = \sum_{l=1}^{N} P_{p,l} \quad P_{in} = \sum_{l=1}^{N} P_{in,l} \tag{7}$$

By subtracting Equations (1)–(2) from Equations (5)–(6), we get the equations that describe the propagation of the low-intensity input wave under the presence of the high-intensity pump wave as follows

$$\nabla^2 (E_{in}) - \mu_0 \varepsilon_\infty \frac{\partial^2 (E_{in})}{\partial t^2} = \mu_0 \sigma \frac{\partial (E_{in})}{\partial t} + \mu_0 \frac{d^2 (P_{in})}{\partial t^2} \tag{8}$$

$$\frac{d^2 (P_{in,l})}{dt^2} + \gamma_l \frac{d(P_{in,l})}{dt} + \omega_l^2 (P_{in,l}) - \frac{\omega_l^2 ({P_{in,l}}^2 + 2 P_{p,l} P_{in,l})}{Q_l e d} + \frac{\omega_l^2 ({P_{in,l}}^3 + 3 P_{p,l} P_{in,l}^2 + 3 P_{p,l}^2 P_{in,l})}{Q_l^2 e^2 d^2}$$

$$= \frac{Q_l e^2 (E_{in})}{m} \tag{9}$$

During the interaction of the two waves, an *idler harmonic* that mediates the amplification of the input wave is generated via *difference frequency generation*. The intensity of the idler harmonic reinforces input wave amplification, and its time variation is embedded in the time variation of the input wave in Equations (8)–(9).

The configuration of the micro-resonator that will be used in the numerical experiments is as illustrated in Figure 1. The pump wave and low-intensity input wave will be excited (originated) from the optical isolator wall, which is the left wall of the resonator. The right cavity wall is an optical bandpass filter with a passband center frequency that is equal to the desired output frequency of the amplified input wave. The thicknesses of the resonator walls are much larger than 20 nanometers, below which necessitates quantum treatment [39]; therefore, the use of classical concepts will suffice here. The input wave electric field amplitude will be normalized to 1 V/m at $t = 0$ sec, and the pump wave electric field will have a very high amplitude in order to induce nonlinearity and transfer energy to the input wave.

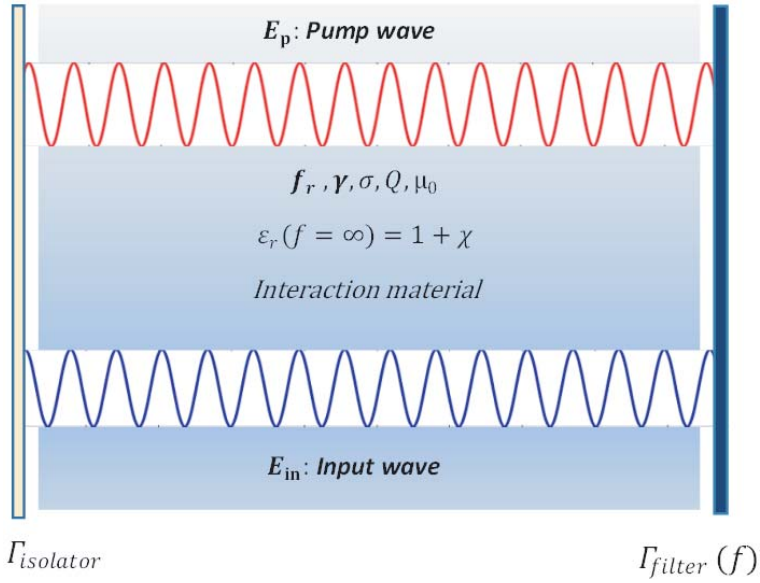

Figure 1. Micro-resonator configuration (Fabry-Perot type) to be used in the numerical simulations.

As we can see from Equations (8)–(9), the pump wave induced polarization density P_p is coupled to the input wave polarization density P_{in}. Therefore, the polarization density induced by the pump wave acts as a coupling coefficient arising from the nonlinearity.

We define the pump wave at the excitation point $x = x_{input}$ to be a combination of M intense ultrashort pulses;

$$E_p\left(x = x_{input}, t\right) = \sum_{i=1}^{M} A_i \cos\left(2\pi\nu_i t + \psi_i\right)\left(u\left(t\right) - u\left(t - \Delta T_i\right)\right) \text{ V/m} \tag{10}$$

$u(t)$: *Unit step function*, ΔT : *Pulse duration*, A : *Amplitude*, ν : *Excitation frequency*

The input wave to be amplified is expressed at the excitation point $x = x_{input}$ as

$$E_{in}(x = x_{input}t) = A_{in}\cos\left(2\pi\left(\nu_{in}\right)t + \psi_{in}\right)\left(u\left(t\right) - u\left(t - \Delta T_{in}\right)\right) \text{V/m} \tag{11}$$

To maximize the gain (or amplitude) of the amplified input wave, we will tune the frequencies $\{\nu_i\}_{i=1,\ldots,M}$ of the ultrashort intense excitation pulses via nonlinear programming using the Fletcher-Reeves algorithm. This algorithm is a nonlinear conjugate gradient algorithm that is well-suited for solving nonlinear programming problems. The cost function F is the absolute value of the input wave spectral density around the desired frequency $v = \nu_{target}$ in a given bandwidth Δv, as indicated in Equation (12)

$$F = |E_{in}(\nu = \nu_{target})| = \left| \int_{\nu_{target}-\Delta\nu/2}^{\nu_{target}+\Delta\nu/2} \left\{ \int_0^{\Delta T} \left\{ E_{in}\left(x = x', t\right) e^{-i(2\pi\Omega)t} \right\} dt \right\} e^{i(2\pi\Omega)t} d\Omega \right| \tag{12}$$

Since our problem is a constrained maximization problem, where the frequencies $\{\nu_i\}_{i=1,\ldots,M}$ can only be tuned in a certain frequency range $\nu_{\min} \leq \{\nu_i\}_{i=1,\ldots,M} \leq \nu_{\max}$, we update the cost function by adding penalty functions to decrease the cost function in case of violation of the constraints, thereby enforcing the satisfaction of the constraints for a maximization based nonlinear programming problem. After the addition of the penalty terms, the cost function for the constrained maximization problem becomes

$$\begin{aligned} F \;=\; |E_{in}(\nu = \nu_{target})| &= \left| \int_{\nu_{target}-\Delta\nu/2}^{\nu_{target}+\Delta\nu/2} \left\{ \int_0^{\Delta T} \left\{ E_{in}\left(x = x', t\right) e^{-i(2\pi\Omega)t} \right\} dt \right\} e^{i(2\pi\Omega)t} d\Omega \right| \\ &- L_1 \left\{ \sum\nolimits_{i=1}^{M} \delta_i (\nu_i - v_{\max})^2 \right\} - L_2 \left\{ \sum\nolimits_{i=1}^{M} \zeta_i \left(\nu_i - v_{\min}\right)^2 \right\} \end{aligned} \tag{13}$$

$\{L_1 L_2\}$: Positive valued penalty constants, $\delta_i \zeta_i$: Penalty coefficients

$$\delta_i = \left\{ \begin{array}{ll} 0 & if \quad \nu_i < v_{\max} \\ > 0 & if \quad \nu_i > v_{\max} \end{array} \right\}, \quad \zeta_i = \left\{ \begin{array}{ll} 0 & if \quad \nu_i > v_{\min} \\ > 0 & if \quad \nu_i < v_{\min} \end{array} \right\} \tag{14}$$

Now that the equations that represent our parametric wave amplification problem are defined, and the corresponding cost function is identified, the optimization algorithm can be introduced. The Fletcher-Reeves algorithm, which is a very convenient algorithm for solving nonlinear programming problems [40], will be used as the optimization algorithm for input wave gain-factor maximization and is explained as follows:

Algorithm: (Fletcher-Reeves)

Given the initial ultrashort pulse frequencies $\mathbf{v_0}$, evaluate the cost function and its gradient: $F_0 = F(\mathbf{v_0})$, $\nabla F_0 = \nabla F(v_0)$. Choose the initial search direction as the identity matrix: $\mathbf{p_0}= \mathbf{I}$.

Set $F_0 \leftarrow \nabla F_0$, $k \leftarrow 0$, and continue the iteration until the gradient is nonzero.

while $\nabla F_k \neq 0$

For each update k, compute the step size α_k using the *backtracking line search*. Choose $0 < c < 1$, $0 < \rho < 1$, and $\alpha_k > 0$. The backtracking line search enables the satisfaction of the *Wolfe conditions* [36] and ensures the stability of the learning rate in a given optimization algorithm [40, 41].

while $F(\mathbf{v_k} + \alpha_k \mathbf{p_k}) \leq F(\mathbf{v_k}) + c\alpha_k \nabla F_k{}^{\mathbf{T}} \mathbf{p_k}$ ($Sufficient\ decrease\ condition$ [36, 42])

$\alpha_k \leftarrow \alpha_k \rho$ (*Keep decreasing* α_k *until the sufficient decrease condition is satisfied*)

end (Terminate the backtracking line search)

set $\mathbf{v_{k+1}} = \mathbf{v_k} + \alpha_k \mathbf{p_k}$, and evaluate ∇F_{k+1}

$$\beta_{k+1} = \frac{\nabla F_{k+1}{}^{\mathbf{T}} \nabla F_{k+1}}{\nabla F_k{}^{\mathbf{T}} \nabla F_k}, \quad \mathbf{p_{k+1}} \leftarrow -\nabla F_{k+1} + \beta_{k+1} \mathbf{p_k}, \quad k \leftarrow k+1;$$

end (Terminate the Fletcher-Reeves algorithm)

The whole procedure for the maximization of the input wave gain-factor, based on the micro-resonator and pump wave parameters, can be summarized as follows

Optimization parameters: $\nu = [\nu_1, \nu_2, \ldots, \nu_M]$, **Cost function to be maximized**: $F(\nu) = |E_{in}(\nu = \nu_{target})|$

Constraints: $\nu_{\min} \leq \nu \leq \nu_{\max}$

Equations: M optimization parameters, $2N + 2$ differential equations, 5 update equations

$$\nabla F_{k-1} = E_{in}(\mathbf{v_{k-1}}) \tag{15}$$

$$\mathbf{v_k} = \mathbf{v_{k-1}} + \alpha_k \mathbf{p_k} \tag{16}$$

$$\nabla^2 (E_p(\mathbf{v_k})) - \mu_0 \varepsilon_\infty \frac{\partial^2 (E_p(\mathbf{v_k}))}{\partial t^2} = \mu_0 \sigma \frac{\partial (E_p(\mathbf{v_k}))}{\partial t} + \mu_0 \frac{d^2 P_p(\mathbf{v_k})}{\partial t^2} \tag{17}$$

$$\frac{d^2 P_{p,l}(\mathbf{v_k})}{dt^2} + \gamma_l \frac{dP_{p,l}(\mathbf{v_k})}{dt} + \omega_l^2 P_{p,l}(\mathbf{v_k}) - \frac{\omega_l^2 P_{p,l}^2(\mathbf{v_k})}{Q_l e d} + \frac{\omega_l^2 P_{p,l}^3(\mathbf{v_k})}{Q_l^2 e^2 d^2} = \frac{Q_l e^2 E_p(\mathbf{v_k})}{m} \tag{18}$$

$$\nabla^2 (E_{in}(\mathbf{v_k})) - \mu_0 \varepsilon_\infty \frac{\partial^2 (E_{in}(\mathbf{v_k}))}{\partial t^2} = \mu_0 \sigma \frac{\partial (E_{in}(\mathbf{v_k}))}{\partial t} + \mu_0 \frac{d^2 (P_{in}(\mathbf{v_k}))}{\partial t^2} \tag{19}$$

$$\begin{aligned} &\frac{d^2 (P_{in,l}(\mathbf{v_k}))}{dt^2} + \gamma_l \frac{d(P_{in,l}(\mathbf{v_k}))}{dt} + \omega_l^2 (P_{in,l}(\mathbf{v_k})) - \frac{\omega_l^2 (P_{in,l}(\mathbf{v_k})^2 + 2P_{p,l}(\mathbf{v_k}) P_{in,l}(\mathbf{v_k}))}{Q_l e d} \\ &+ \frac{\omega_l^2 (P_{in,l}^3(\mathbf{v_k}) + 3P_{p,l}(\mathbf{v_k}) P_{in,l}^2(\mathbf{v_k}) + 3P_{p,l}^2(\mathbf{v_k}) P_{in,l}(\mathbf{v_k}))}{Q_l^2 e^2 d^2} = \frac{Q_l e^2 (E_{in}(\mathbf{v_k}))}{m} \end{aligned} \tag{20}$$

$$\nabla F_k = E_{in}(\mathbf{v_k}), \quad \beta_k = \frac{\nabla F_k{}^{\mathbf{T}} \nabla F_k}{\nabla F_{k-1}{}^{\mathbf{T}} \nabla F_{k-1}}, \quad \mathbf{p_k} \leftarrow -\nabla F_k + \beta_k \mathbf{p_{k-1}}, \quad k \leftarrow k+1, \quad l = 1, \ldots, N \tag{21}$$

***FDTD Discretization*:** Equations (17)–(20) are discretized and solved using the finite difference time domain method at every update of the nonlinear programming process. Since the problem is nonlinear, the stability condition is stricter; therefore, it is the best to choose the temporal and spatial

sampling periods $(\Delta t, \Delta x)$ as small as possible for more accurate solutions. The discretization of Equations (17)–(20) is performed respectively as follows

Equations for the pump wave:

$$\frac{E_{p,k}(i+1,j)-2E_{p,k}(i,j)+E_{p,k}(i-1,j)}{\Delta x^2}-\mu_0\varepsilon_\infty(i,j)\frac{E_{p,k}(i,j+1)-2E_{p,k}(i,j)+E_{p,k}(i,j-1)}{\Delta t^2}$$
$$=\mu_0\sigma(i,j)\frac{E_{p,k}(i,j)-E_{p,k}(i,j-1)}{\Delta t}+\mu_0\frac{P_{p,k}(i,j+1)-2P_{p,k}(i,j)+P_{p,k}(i,j-1)}{\Delta t^2} \quad (22)$$

$$\frac{P_{pl,k}(i,j+1)-2P_{pl,k}(i,j)+P_{pl,k}(i,j-1)}{\Delta t^2}+\gamma_l\frac{P_{pl,k}(i,j)-P_{pl,k}(i,j-1)}{\Delta t}+4\pi^2 f_l^2\left(P_{pl,k}(i,j)\right)$$
$$-\frac{4\pi^2 f_l^2}{Q_l e d}\left(P_{pl,k}(i,j)\right)^2+\frac{4\pi^2 f_l^2}{Q_l^2 e^2 d^2}\left(P_{pl,k}(i,j)\right)^3=\frac{Q_l e^2}{m}\left(E_{p,k}(i,j)\right) \quad (23)$$

Equations for the input wave:

$$\frac{E_{in,k}(i+1,j)-2E_{in,k}(i,j)+E_{in,k}(i-1,j)}{\Delta x^2}-\mu_0\varepsilon_\infty(i,j)\frac{E_{in,k}(i,j+1)-2E_{in,k}(i,j)+E_{in,k}(i,j-1)}{\Delta t^2}$$
$$=\mu_0\sigma(i,j)\frac{E_{in,k}(i,j)-E_{in,k}(i,j-1)}{\Delta t}+\mu_0\frac{E_{in,k}(i,j+1)-2E_{in,k}(i,j)+E_{in,k}(i,j-1)}{\Delta t^2} \quad (24)$$

$$\frac{P_{inl,k}(i,j+1)-2P_{inl,k}(i,j)+P_{inl,k}(i,j-1)}{\Delta t^2}+\gamma_l\frac{P_{inl,k}(i,j)-P_{inl,k}(i,j-1)}{\Delta t}+4\pi^2 f_l^2\left(P_{inl,k}(i,j)\right)$$
$$-\frac{4\pi^2 f_l^2}{Q_l e d}\left\{\left(P_{inl,k}(i,j)\right)^2+2P_{inl,k}(i,j)\,P_{pl,k}(i,j)\right\}+\frac{4\pi^2 f_l^2}{Q_l^2 e^2 d^2}\left\{\left(P_{inl,k}(i,j)\right)^3+3\left(P_{inl,k}(i,j)\right)^2 P_{pl,k}(i,j)\right.$$
$$\left.+3P_{inl,k}(i,j)\left(P_{pl,k}(i,j)\right)^2\right\}=\frac{Q_l e^2}{m}\left(E_{in,k}(ij)\right) \quad (25)$$

$$P_{p,k}=P_{p1,k}+P_{p2,k}+\ldots+P_{pN,k},\quad P_{in,k}=P_{in1,k}+P_{in2,k}+\ldots+P_{inN,k} \quad (26)$$

x: Space point, t: Time instant, k: update number, $E_k(x,t)=E_k(i\Delta x, j\Delta t)\rightarrow E_k(i,j)$

$E_{p,k}$: *Pump wave electric field at update k*, $E_{in,k}$: *Input wave electric field at update k*

The summary of the whole process is illustrated as a flowchart diagram in Figure 2 given below.

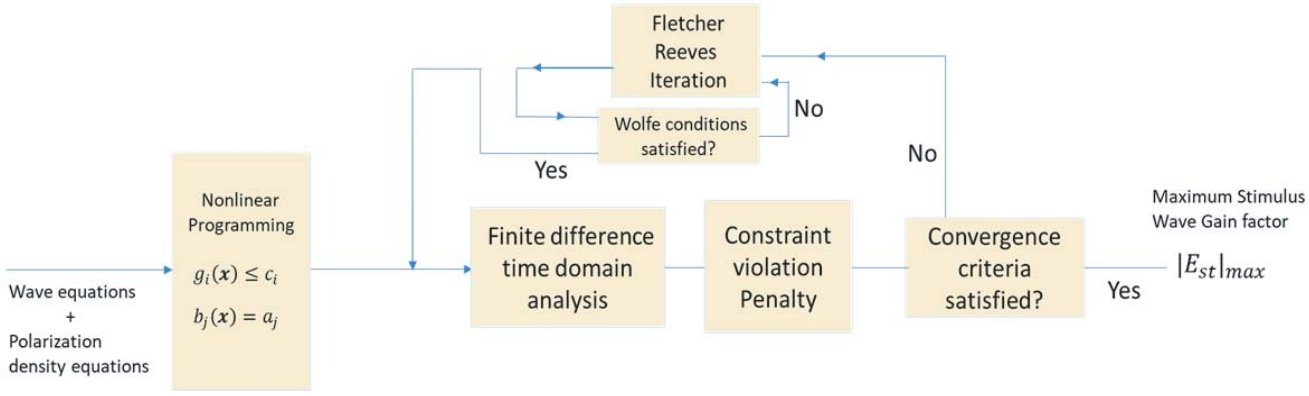

Figure 2. The flowchart summary of the nonlinear programming problem.

3. SIMULATION RESULTS

The configuration of the micro-resonator, which will be studied in the upcoming simulation results, is presented as in Figure 3. The left wall of the resonator is an optical isolator that allows an optical pulse to pass from its left side and blocks any transmission of the pulse from its right side. The right cavity

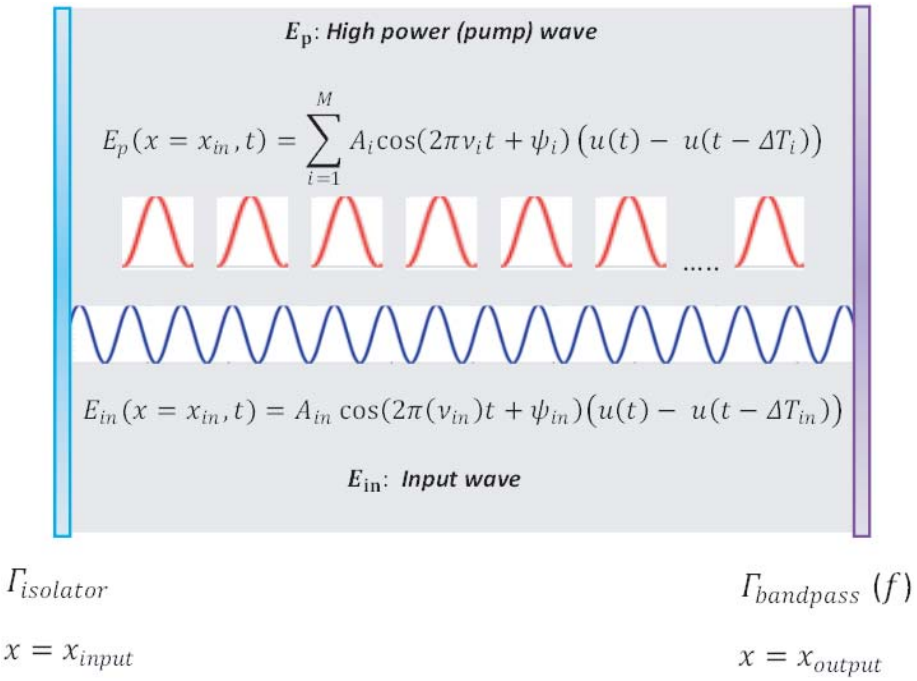

Figure 3. Configuration of the cavity.

wall is an optical bandpass filter that allows the transmission of the input wave at the desired frequency and reflects all the other frequency components. The cavity walls are assumed to yield no reflection loss, and the cavity round-trip loss here is solely due to the polarization damping coefficients of the gain medium. This is an accurate assumption because the effect of the polarization damping loss is much more significant than the reflection loss [20], as the polarization damping loss decreases both the rate of electric energy coupling and the intracavity stored electric energy, which are critical for input wave OPA gain [37].

The general conditions and configuration of the presented numerical simulations is outlined below

$$\textit{Optical isolator location (left wall)}:\ x = 0\,\mu\text{m};\quad \textit{Bandpass filter (right wall) location}:\ x = 10\,\mu\text{m}$$

$$\textit{Interaction medium range}:\ 0\,\mu\text{m} < x < 10\,\mu\text{m};\ \textit{Number of electrons per volume}:\ N = 3.5\times10^{28}/\text{m}^3$$

$$\textit{Atomic diameter}:\ d = 0.3\,\textit{nanometers}$$

Optical isolator condition: Full reflection at $x = x_{input}$ from the inside of the cavity

$$\Gamma(x = x_{input} - \Delta x, t){=}0,\quad \Gamma(x = x_{input} + \Delta x, t){=}1,\ (\Gamma:\ \textit{Reflection coefficient})$$

Optical bandpass filter condition: Frequency dependent reflection at $x = x_{output}$; $|\Gamma(\nu)| = 1 - e^{-\left(\frac{(\nu-\nu')}{\sqrt{2\Delta\nu^2}\,\text{THz}}\right)^2}$ ($\textit{Full transmission around}\nu = \nu'$); $\Delta\nu$: Transmission bandwidth of the bandpass filter

Initial conditions: (Prime sign represents the time derivative)

$$P_p(x,0) = P'_p(x,0) = E_p(x,0) = E'_p(x,0) = P_{in}(x,0) = P'_{in}(x,0) = E_{in}(x,0) = E'_{in}(x,0) = 0$$

Absorbing boundary condition (perfectly matched layer): Gradually increased electrical conductance for the effective termination of the computational domain

$$\sigma(x) = \left\{ \begin{array}{l} (x - (L - \Delta))\sigma_0\,, \quad (L - \Delta) \le x < L \end{array} \right\},\ for\ L = 15\,\mu\text{m},\ \Delta = 2.5\,\mu\text{m},\ \sigma_0 = 4.5\times10^8\,\text{S/m}$$

The value of σ_0 is determined based on the thickness of the perfectly matched layer using the given formula

$$\sigma_0 = \frac{\textit{Center wavelength of the simulation spectral band}}{\Delta x^2} \tag{27}$$

Note that the absorbing boundary condition is required to terminate the computational domain from the right side. Since the left side is already a closed boundary due to the full reflection from the optical isolator, an absorbing boundary condition is not imposed from the left side.

3.1. Simulation1: Blue Light Amplification

Problem definition: Identifying the optimal excitation frequencies of the ultrashort pulses of the pump wave $\{\nu_i\}_{i=1,2}$ in order to maximize the absolute value of the peak amplitude of the input wave at 640 THz ($|E_{in}(v_{in}=640\,\text{THz})|$) inside the cavity, for $100\,\text{THz} < \{\nu_i\}_{i=1,2} < 400\,\text{THz}$, and for $\mu\text{m} < x < 10\,\mu\text{m}$, $0 \le t \le 15\,\text{ps}$. The parameters of the micro-resonator and the parameters of the input and pump waves at the excitation point are presented below $E_{in}(x = x_{input} = 2.5\,\mu\text{m}, t) = 1 \times \frac{\sin(2\pi(6.4\times10^{14})t)\,V}{m}$, $0 \le t \le 15\,\text{ps}$, $E_p(x = x_{input} = 2.5\,\mu\text{m}, t) = \sum_{i=1}^{2} A_i \cos(2\pi\nu_i t + \psi_i)(u(t) - u(t - \Delta T_i))\,\text{V/m}$

$A_1 = 1\times10^8$, $A_2 = 8\times10^7$, $\Delta T_1 = 5\,\text{ps}$, $\Delta T_2 = 8\,\text{ps}$; *Spatial and temporal parameters* : $0 \le x \le 10\,\mu\text{m}$, $0 \le t \le 15\,\text{ps}$, *Cavity resonances* : $\mathbf{f_r} = \{3.8\times10^{14}\,\text{Hz}, 5.4\times10^{14}\,\text{Hz}, 7.5\times10^{14}\,\text{Hz}\}$; *Damping rates of the cavity* : $\gamma = \{5\times10^{11}\,\text{Hz}, 1\times10^{12}\,\text{Hz}, 3\times10^{12}\,\text{Hz}$; *Resonator (oscillator) strengths* $= \xi = f\frac{3}{9}, \frac{4}{9}, \frac{2}{9}\}$, *Relative permittivity* : $(\varepsilon_r) = 10 \quad (\mu_r = 1)$.

Since we want the input wave intensity to be maximized around 640 THz (blue light emission), the unconstrained cost function is determined as $F = Gain = |E_{in}(v_{in} = 640\,\text{THz})| = |\int_{6.4\times10^{14}-\Delta\nu}^{6.4\times10^{14}+\Delta\nu} \{\int_0^{\Delta T} \{E_{in}(x = x', t)e^{-i(2\pi\Omega)t}\}dt\}e^{i(2\pi\Omega)t}d\Omega|$, $\Delta T = 15\,\text{ps}(6.4\times10^{14} - \Delta\nu)\,\text{Hz} < \Omega < (6.4\times10^{14} + \Delta\nu)\,\text{Hz}$, $\Delta\nu = 10\,\text{THz}$.

Optical bandpass filter condition: Frequency dependent reflection at $x = 10\,\mu\text{m}$. The passband of the filter is centered at 640 THz (blue light filter) and has a Gaussian frequency selectivity curve with a bandwidth of 20 THz.

$$\left|\Gamma\left(\nu'\right)\right| = 1 - e^{-\left(\frac{(\nu' - 640THz)}{\sqrt{200\,\text{THz}}}\right)^2}$$

Constrained cost function: Since the allowed range of ultrashort excitation frequencies lies in the range $100\,\text{THz} < \{\nu_i\}_{i=1,2} < 400\,\text{THz}$, the cost function is modified to include the penalty terms for constraint breaches. Therefore, the cost function to be maximized for this problem is finalized as

$$\begin{aligned} F(\nu_1, \nu_2) &= |E_{in}(v_{in} = 640\,\text{THz})| - \delta_1 (v_1 - 400\,\text{THz})^2 - \delta_2 (100\,\text{THz} - v_1)^2 \\ &\quad -\delta_3 (v_2 - 400\,\text{THz})^2 - \delta_4 (100\,\text{THz} - v_2)^2; \end{aligned}$$

Parameter values for $\{\delta_i\}_{i=1,2,3,4}$: $\zeta = 1.5$, $\Delta\Omega = 10\,\text{THz}$, *such that*

$$\delta_1 = \left\{ \begin{array}{ll} 0, & if \quad v_1 \le 400\,\text{THz} \\ \dfrac{\left(1 - \frac{1}{\zeta}\right)}{(\Delta\Omega)^2} |E_{in}(v_{in} = 640\,\text{THz})|, & if \quad v_1 > 400\,\text{THz} \end{array} \right\},$$

$$\delta_2 = \left\{ \begin{array}{ll} 0, & if \quad v_1 \ge 100\,\text{THz} \\ \dfrac{\left(1 - \frac{1}{\zeta}\right)}{(\Delta\Omega)^2} |E_{in}(v_{in} = 640\,\text{THz})|, & if \quad v_1 < 100\,\text{THz} \end{array} \right\}$$

$$\delta_3 = \left\{ \begin{array}{ll} 0 & if \quad v_2 \le 400\,\text{THz} \\ \dfrac{\left(1 - \frac{1}{\zeta}\right)}{(\Delta\Omega)^2} |E_{in}(v_{in} = 640\,\text{THz})|, & if \quad v_2 > 400\,\text{THz} \end{array} \right\},$$

$$\delta_4 = \left\{ \begin{array}{ll} 0 & if \quad v_2 \ge 100\,\text{THz} \\ \dfrac{\left(1 - \frac{1}{\zeta}\right)}{(\Delta\Omega)^2} |E_{in}(v_{in} = 640\,\text{THz})|, & if \quad v_2 < 100\,\text{THz} \end{array} \right\}$$

ζ = *Reduction factor*, $\Delta\Omega$: *Deviation from the* max / min *allowable frequency*

which indicates that the cost function is reduced by $(100 - \frac{100}{\zeta})\%$ for a frequency deviation of $\Delta\Omega$, for each penalty coefficient. Based on this configuration, the maximization process of the cost function is summarized in Table 1.

Table 1. Optimization process (Fletcher-Reeves algorithm).

ν_1	ν_2	$Gain_{\max}$	$W_{e,p}$ (J/m^3)	$P_p(C/m^2)$	k (iteration #)
270 THz	260.0 THz	1.23	1.5×10^7	0.12	1
241.6 THz	252.8 THz	1.29	2.9×10^7	0.13	5
218.9 THz	278.2 THz	41.84	4.4×10^7	0.13	9
238.5 THz	288.1 THz	117.51	6.9×10^7	0.14	13
204.5 THz	302.2 THz	3255.34	9.2×10^7	0.16	17
198.4 THz	311.6 THz	5287.14	1.5×10^8	0.16	21
172.4 THz	288.5 THz	1.46×10^4	2.8×10^8	0.18	25
187.0 THz	323.1 THz	2.16×10^5	8.8×10^8	0.20	29
156.6 THz	349.7 THz	8.73×10^5	9.7×10^8	0.22	33
164.8 THz	352.4 THz	5.68×10^6	1.6×10^9	0.24	37
162.3 THz	351.3 THz	3.30×10^7	3.0×10^9	0.26	40
161.7 THz	350.9 THz	4.7×10^7	3.1×10^9	0.27	42

As illustrated in Table 1, the gain factor of the input wave at the desired frequency is proportional to the intracavity electric energy density $W_{e,p}$ and the polarization density P_p induced by the pump wave. Therefore, we conclude that the input wave gain-factor maximization problem is equivalent to the concurrent maximization of the intracavity electric energy density and the corresponding polarization density, created by the pump wave. This is expected, as the accumulated polarization density signifies the strength of nonlinear coupling and is the sole parameter or mechanism that enables the transfer of energy from the energized cavity to the input wave (see Equations (8), (9)). Hence, maximizing the electric energy alone is not sufficient to amplify the input wave, and the simultaneous maximization of the coupling coefficient (pump wave induced polarization density) is also necessary. Both the intracavity electric energy density and the polarization density induced by the pump wave can be maximized by maximizing the nonlinear constructive interference of the pump wave. Therefore, in its essence the algorithm seeks to maximize nonlinear constructive interference based on the excitation frequencies of the ultrashort pulses. The algorithm is especially useful in cases where the cavity is energized by many ultrashort pulses, such as the output pulses of a mode-locked laser. This is because as the number of ultrashort pulses increases, the algorithm has more freedom for a fine tuning, and a given gain factor for the input wave can be achieved at a lower ultrashort pulse mean-amplitude. On the other hand, as the number of the ultrashort pulses increases, the algorithm takes much more time to maximize the gain factor of the input wave. In this simulation with two ultrashort pulses, a high-gain amplification is achieved at the 42nd update.

Figure 4 displays the amplification of the input wave around the desired frequency (quasi-monochromatic with a bandwidth of 20 THz) corresponding to the optimal frequencies of the ultrashort pulses which leads to the optimal pump wave excitation. A very high gain-factor is achieved at the filter output after 15 picoseconds. The amplitude of the input wave increases significantly after $t = 10$ picoseconds due to the exponential rate of amplification, in compliance with the theoretical results reported in [34, 35].

3.2. Simulation2: Infra-Red (IR) Light Amplification

Problem definition: Identification of the optimal excitation frequency of the pump wave ν_p in order to maximize the absolute value of the peak amplitude of the input wave at 100 THz ($|E_{in}(\upsilon_{in} = 100\,\text{THz})|$)

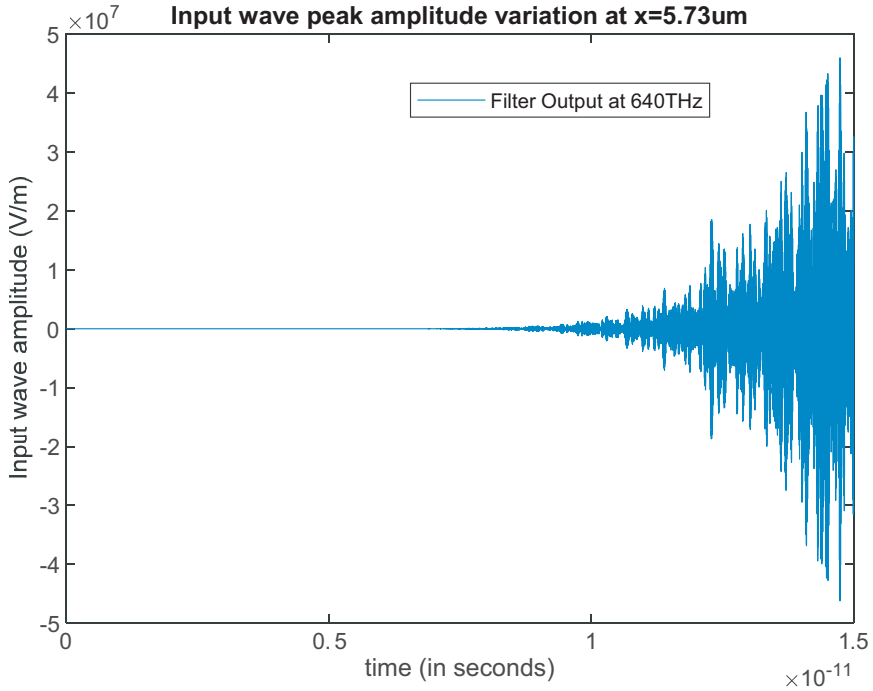

(a)

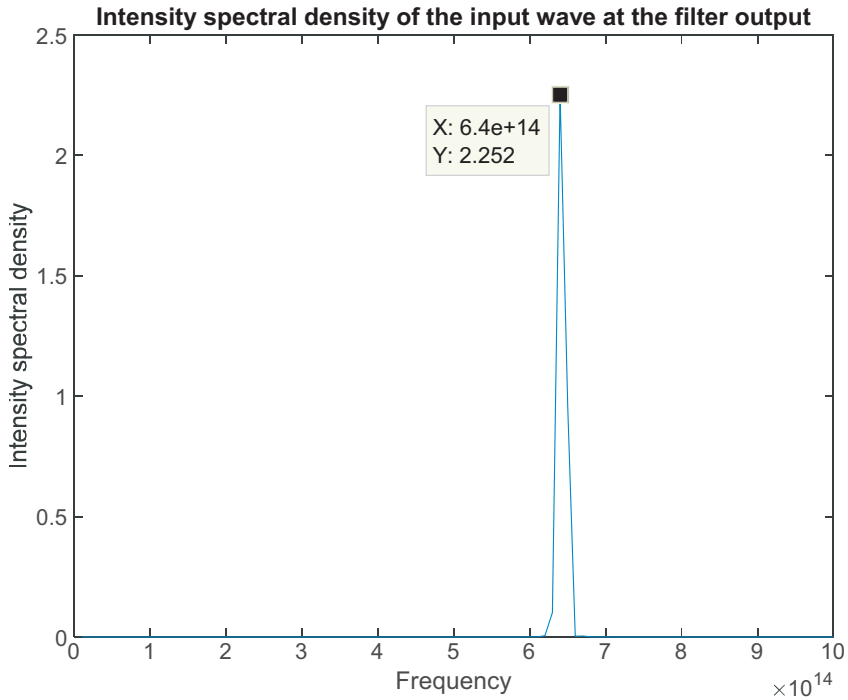

(b)

Figure 4. (a) Amplitude variation of the input wave w.r.t time at the bandpass filter output. (b) Input wave intensity spectral density measured at the bandpass filter output.

inside the micro-resonator, for a constrained tuning range of $100\,\text{THz} < \nu_p < 400\,\text{THz}$, for $\mu\text{m} < x < 10\,\mu\text{m}$, $0 \leq t \leq 20\,\text{ps}$. The parameters of the micro-resonator and the parameters of the input and pump waves at the excitation point are presented below (note that in this case the pump wave excitation is a

single pulse, whose pulse duration is equal to the pulse duration of the input wave)

$$\begin{aligned}
E_{in}(x = x_{input} = 2.5\,\mu\text{m}t) &= 1 \times \sin\left(2\pi\left(1 \times 10^{14}\right)t\right)\ \text{V/m},\\
E_p\left(x = x_{input} = 2.5\,\mu\text{m}, t\right) &= 1.8 \times 10^8 \cos\left(2\pi(v_p)t + \psi_p\right)\ \text{V/m},\\
\textit{Spatial and temporal parameters}: &\quad 0 \le x \le 10\,\mu m,\ 0 \le t \le 20\,\text{ps},\ \psi_p = 0\\
\textit{Cavity resonances}: &\quad \mathbf{f_r} = \{1.1 \times 10^{15}\,\text{Hz},\ 1.5 \times 10^{15}\,\text{Hz},\\
\textit{Damping rates of the cavity}: &\quad \gamma = \{2 \times 10^{12}\,\text{Hz},\ 5 \times 10^{12}\,\text{Hz},\\
\textit{Resonator (oscillator) strengths} &= \xi = f\frac{1}{2},\ \frac{1}{2}g,\\
\textit{Relative permittivity}: &\quad (\varepsilon_r) = 12 \quad (\mu_r = 1)
\end{aligned}$$

Since we want the input wave intensity to be maximized around 100 THz (IR light emission), the unconstrained cost function is determined as

$$F = \left|E_{in}\left(v_{in} = 100\,\text{THz}\right)\right| = \left|\int_{1\times10^{14}-\Delta v}^{1\times10^{14}+\Delta v}\left\{\int_0^{\Delta T}\left\{E_{in}(x = x', t)e^{-i(2\pi\Omega)t}\right\}dt\right\}e^{i(2\pi\Omega)t}d\Omega\right|$$

$$\Delta T = 20\,\text{ps} \left(1 \times 10^{14} - \Delta v\right)\ \text{Hz} < \Omega < \left(1 \times 10^{14} + \Delta v\right)\ \text{Hz},\ \Delta v = 5\,\text{THz}$$

Optical bandpass filter condition: Frequency dependent reflection at $x = 10\,\mu\text{m}$. The passband of the filter is centered at 100 THz (IR light filter) and has a Gaussian frequency selectivity curve with a bandwidth of 10 THz.

$$\left|\Gamma\left(v'\right)\right| = 1 - e^{-\left(\frac{\left(v' - 100\ \text{THz}\right)}{\sqrt{50\ \text{THz}}}\right)^2}$$

Constrained cost function: Since the allowed pump wave frequencies lie in the range $100\,\text{THz} < \nu_p < 400\,\text{THz}$, the cost function is modified to include the penalty terms for constraint breaches. Therefore, the cost function to be maximized for this problem is finalized as

$$\begin{aligned}
&F\left(v_p\right) = \left|E_{in}\left(v_{in} = 100\,\text{THz}\right)\right| - \delta_1\left(v_p - v_{\max}\right)^2 - \delta_2\left(v_{min} - v_p\right)^2,\\
&Parameter\ values\ for\ \{\delta_i\}_{i=1,2}:\ \ \zeta = 2,\ \ \Delta\Omega = 3\,\text{THz},\quad such\ that\\
&\delta_1 = \left\{\begin{array}{ll} 0, & if \quad v_p \le 400\,\text{THz}\\ \dfrac{\left(1 - \frac{1}{\zeta}\right)}{\left(\Delta\Omega\right)^2}\left|E_{in}\left(v_{in} = 100\,\text{THz}\right)\right|, & if \quad v_p > 400\,\text{THz}\end{array}\right\},\\
&\delta_2 = \left\{\begin{array}{ll} 0, & if \quad v_p \ge 100\,\text{THz}\\ \dfrac{\left(1 - \frac{1}{\zeta}\right)}{\left(\Delta\Omega\right)^2}\left|E_{in}\left(v_{in} = 100\,\text{THz}\right)\right|, & if \quad v_p < 100\,\text{THz}\end{array}\right\}
\end{aligned}$$

Based on this configuration, the maximization process of the cost function is summarized in Table 2. From Table 2, we can see that the gain factor of the input wave at the desired frequency is proportional to the intracavity electric energy density $W_{e,p}$ and the polarization density P_p induced by the pump wave. Once again, we deduce that the input wave gain-factor maximization problem is equivalent to the concurrent maximization of the intracavity electric energy density and the corresponding polarization density, created by the pump wave. The highest gain factor is achieved at the 28th update, indicating a fair convergence rate.

Figure 5 displays the amplification of the input wave around the desired frequency (quasi-monochromatic with a bandwidth of 10 THz) for the optimal excitation frequency of the pump wave. A very high gain-factor is achieved at the filter output after 20 picoseconds. The amplitude of the input wave increases significantly after $t = 10$ picoseconds, when the accumulated intracavity energy becomes sufficiently high.

Table 2. Optimization process (Fletcher-Reeves algorithm).

ν_p	$Gain_{\max}$	$W_{e,p}$ $(\frac{J}{m^3})$	$P_{pump}(\frac{C}{m^2})$	k (iteration #)
225.0 THz	13.2	2.4×10^7	0.14	1
257.0 THz	17.7	2.5×10^7	0.16	4
260.1 THz	83.4	2.7×10^7	0.17	7
262.5 THz	196.0	4.1×10^7	0.19	10
264.6 THz	1271.6	4.9×10^7	0.20	12
259.5 THz	6350.8	6.6×10^7	0.22	14
227.3 THz	2.6×10^4	9.3×10^7	0.23	16
83.3 THz	5.3×10^4	1.1×10^8	0.25	18
143.3 THz	3.7×10^5	2.8×10^8	0.26	20
158.0 THz	1.2×10^6	3.7×10^8	0.28	22
166.9 THz	8.4×10^6	1.0×10^9	0.29	24
152.9 THz	4.1×10^7	2.2×10^9	0.30	26
157.4 THz	1.5×10^8	3.2×10^9	0.31	28

4. MODEL VALIDATION

The accuracy of the computational model presented in this study is tested using the available experimental formula for harmonic generation by nonlinear wave mixing, which involves the generation of a new harmonic (angular frequency: ω_3) through the mixing of two monochromatic high-intensity waves (with angular frequencies ω_1 and ω_2) in a strongly nonlinear medium, such that the newly generated harmonic is the sum of the two intermixed harmonics ($\omega_3 = \omega_1 + \omega_2$). For a simulation duration of $0 \leq t \leq t_{\max}$, the numerical expression for *sum harmonic (frequency) generation efficiency* is given as

$$\begin{aligned} \eta_{numerical} &= \frac{\text{Intensity of the new } \omega_3 \text{ harmonic of the total wave at } x = x''}{\text{Intensity of the } \omega_2 \text{ harmonic of the total wave at } x = x''} \\ &= \frac{\left| \int_0^{\Delta T} \{E(x = x'', t) e^{-i(2\pi f_3)t}\} dt \right|^2}{\left| \int_0^{\Delta T} \{E(x = x'', t) e^{-i(2\pi f_2)t}\} dt \right|^2} \end{aligned} \tag{28}$$

Since both waves are of high-intensity, and our aim is not amplification, we can treat the total wave like a pump wave and obtain the numerical efficiency (Equation (30)) by solving the discretized equations for the pump wave (Equations (24)–(25)). The experimental formula for sum-harmonic generation efficiency is given as

$$\eta_{experimental} = \frac{\omega_3}{\omega_2} \left(\sin \sqrt{2 d^2 \eta^3 \omega_3^2 \left(cn\varepsilon_0 A_2^2 \right) L^2} \right)^2 \text{ [34, 35, 43–45]} \tag{29}$$

d = Strength of Nonlinearity, η = Intrinsic impedance, n = Refractive index, A_2 = Amplitude of the pump wave, A_1 = Amplitude of the signal, L = Interaction (medium) length, $\omega_3 = \omega_1 + \omega_2$ = Frequency of the sum harmonic.

In order to compute and compare the numerical and experimental efficiencies, a 180 THz high-intensity wave $\mathbf{E_2}$ is intermixed with a 120 THz high-intensity wave $\mathbf{E_1}$ (see Figure 6). The amplitudes

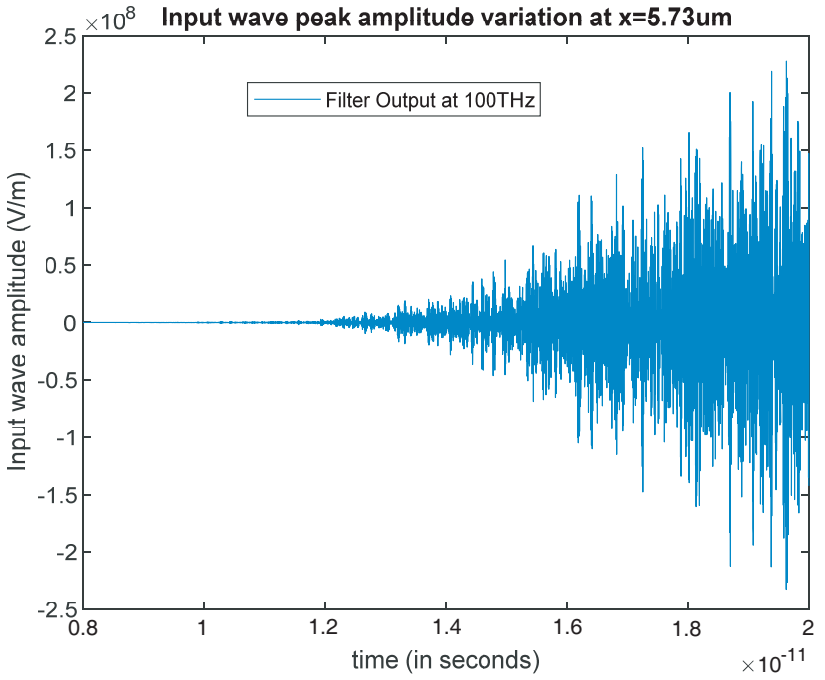

(a)

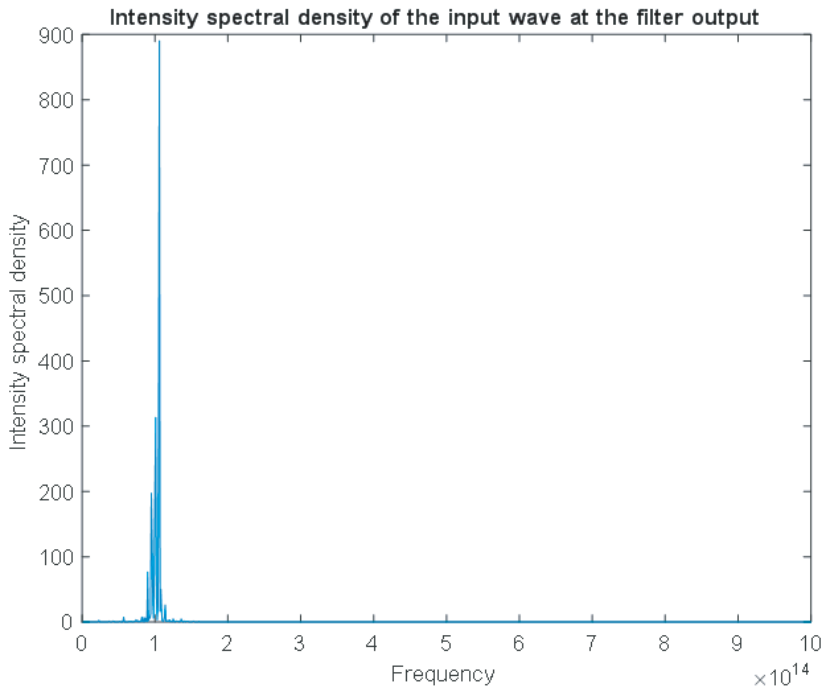

(b)

Figure 5. (a) Amplitude variation of the input wave w.r.t time at the bandpass filter output. (b) Input wave intensity spectral density measured at the bandpass filter output.

of the waves are A_2 and A_1, respectively, and the parameters of the medium are as given below

$$\mathbf{E_2}(x = 2.6\,\mu\mathrm{m}\,t) = A_2 \times \sin\left(2\pi\left(1.8 \times 10^{14}\right)t + \varphi_2\right)\ \mathrm{V/m};$$

$$\mathbf{E_1}(x = 2.6\,\mu\mathrm{m}\,t) = A_1 \times \sin\left(2\pi\left(1.2 \times 10^{14}\right)t + \varphi_1\right)\ \mathrm{V/m}\,(\varphi_1 = 0,\ \varphi_2 = 0);$$

Spatial and temporal simulation parameters : $0 \le x \le 10\,\mu\mathrm{m},\ 0 \le t \le 30\,\mathrm{ps}$;

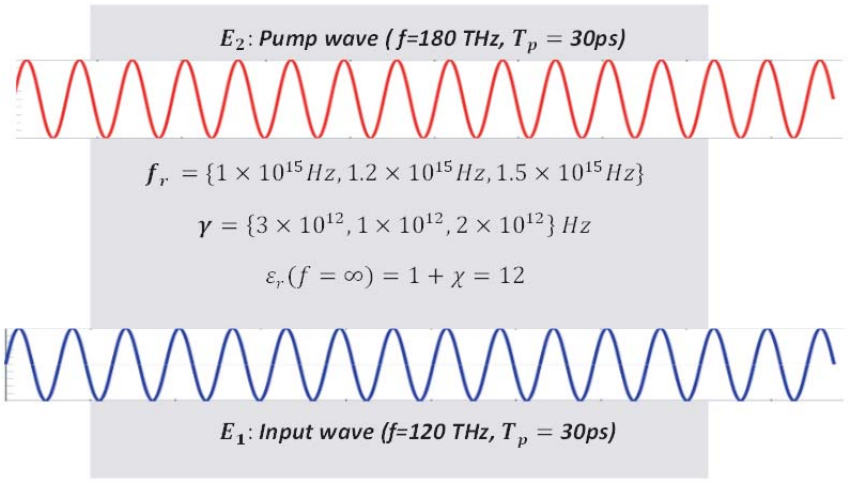

Figure 6. Configuration for sum-frequency generation.

$$\begin{aligned}
&\textit{Resonance frequencies of the medium}: \mathbf{f_r} = \{1 \times 10^{15}\,\text{Hz},\ 1.2 \times 10^{15}\,\text{Hz},\ 1.5 \times 10^{15}\,\text{Hz};\\
&\textit{Damping (decay) rates of the medium}: \gamma = \left\{3 \times 10^{12}\,\text{Hz},\ 1 \times 10^{12}\,\text{Hz},\ 2 \times 10^{12}\,\text{Hz}\right\};\\
&\textit{Permittivity of the medium}\,(\varepsilon_\infty) = 1 + \chi = 12 \ \ (\mu_r = 1)
\end{aligned}$$

The values of each parameter involved in the process are as stated below:

$$\begin{aligned}
\omega_2 &= \textit{Second wave angular frequency} = (2\pi \times 180)\,\text{THz},\\
\omega_1 &= \textit{First wave angular frequency} = (2\pi \times 120)\,\text{THz},\\
L &= \textit{Cavitymedium length} = 3.33\,\mu\text{m},
\end{aligned}$$

$$\begin{aligned}
\omega_3 &= \textit{Sum harmonic angular frequency} = 2\pi \times 300\,\text{THz}, \quad n = \sqrt{12},\\
A_2 &= \textit{Amplitude of the second wave}(\textit{Swept from}\,1 \times 10^8\,\text{V/m}\ \textit{to}\ 2.5 \times 10^9\,\text{V/m}),\\
A_1 &= \textit{Amplitude of the first wave} = A_2/10,\\
&\textit{Resonator (oscillator) strengths} = \xi = \left\{\frac{1}{3}, \frac{1}{3}, \frac{1}{3}\right\}
\end{aligned}$$

The nonlinearity coefficient is estimated by equating the numerical and theoretical efficiencies for a sample pump wave amplitude (preferably at a very high pump wave amplitude for a more reliable estimation). At a sample pump wave amplitude of $A_2 = 10^9\,\text{V/m}$, the numerical efficiency is found as $\eta_{numerical} = 3.7 \times 10^{-4}$. Based on the given parameters, by equating the numerical and experimental efficiencies at the sample pump wave amplitude of $A_2 = 10^9\,\text{V/m}$, we can solve the nonlinearity coefficient;

$$\eta_{\text{exp}} = \frac{\omega_3}{\omega_2}\left(\sin\sqrt{2{d_{est}}^2\eta^3\omega_3^2(cn\varepsilon_0 A_2^2)L^2}\right)^2 = \eta_{num} = 3.7 \times 10^{-4},$$

from which we solve the estimated nonlinearity coefficient as $d_{est} = 3.31 \times 10^{-23}$. Since this estimated nonlinear coefficient is based on a single sample pump wave amplitude, we must double check its accuracy by comparing the efficiencies for some other sample pump wave amplitudes. This comparison is shown in Table 3. Since the mean error percentage is low, the nonlinearity coefficient is accurately estimated.

Finally, we compare the numerical and experimental efficiencies for a much larger sample of pump wave amplitudes swept from $1 \times 10^8\,\text{V/m}$ to $2.5 \times 10^9\,\text{V/m}$ in increments of $0.5 \times 10^8\,\text{V/m}$. The comparison is plotted in Figure 7. The results are in good agreement, and the mean error percentage is below 0.7%.

Table 3. Comparing numerical and experimental sum-harmonic generation efficiencies for the nonlinearity coefficient of $d_{est} = 3.31 \times 10^{-23}\,\mathrm{C/V^2}$.

Pump wave Amplitude	Experimental efficiency	Numerical efficiency	Error percentage
$1 \times 10^8\,\mathrm{V/m}$	4.16×10^{-6}	4.22×10^{-6}	1.4%
$3 \times 10^8\,\mathrm{V/m}$	3.36×10^{-5}	3.40×10^{-5}	1.2%
$5 \times 10^8\,\mathrm{V/m}$	9.25×10^{-5}	9.27×10^{-5}	0.22%
$1 \times 10^9\,\mathrm{V/m}$	3.68×10^{-4}	3.70×10^{-4}	0.54%
$1.5 \times 10^9\,\mathrm{V/m}$	8.32×10^{-4}	8.25×10^{-4}	0.85%
$2 \times 10^9\,\mathrm{V/m}$	1.48×10^{-3}	1.48×10^{-3}	0.31%
$2.5 \times 10^9\,\mathrm{V/m}$	2.31×10^{-2}	2.33×10^{-2}	0.96%

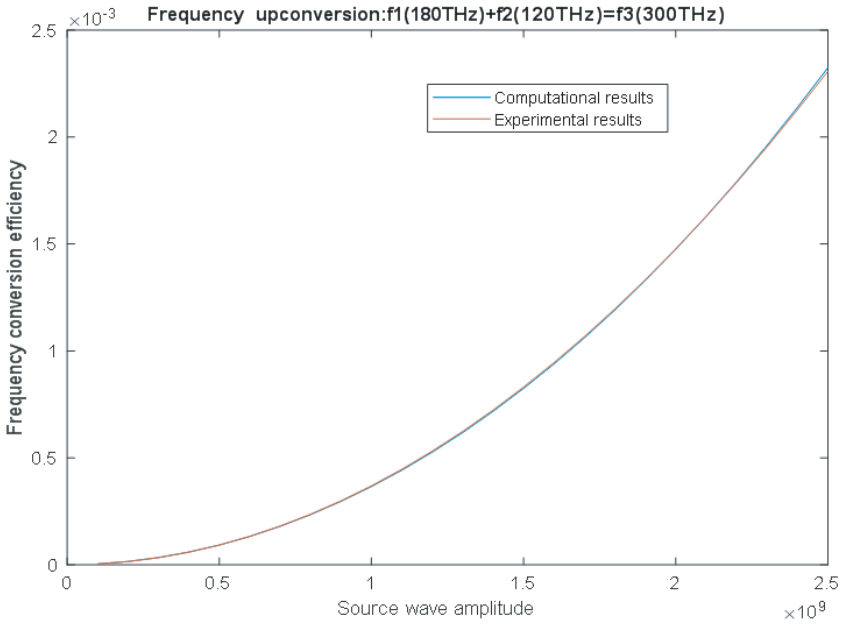

Figure 7. Comparison of sum-harmonic generation efficiencies for $f_3 = 300\,\mathrm{THz}$ and $d = 3.31 \times 10^{-22}\,\mathrm{C/V^2}$.

5. CONCLUSION

Here we have presented an efficient algorithm that maximizes the energy transfer from the pump wave to the input wave and enable the amplification of an input wave within a Fabry-Perot micro-resonator via optical parametric amplification. In a simple micro-resonator with an arbitrary interaction medium, the intense excitation pulses that comprise the pump wave can be tuned or programmed to maximize the optical gain of an input wave through the nonlinear wave mixing process. The Fletcher-Reeves algorithm can be employed for tuning the frequencies of the excitation pulses generated by the source device, based on the configuration of the optical micro-resonator through a micro-controller interface between the micro-resonator and the source device. The algorithm allows for high-gain wave amplification at a desired optical frequency and at the minimal threshold pump wave energy, for a given micro-resonator configuration with an interaction medium of multiple resonance frequencies. The computational results of our formulations match the well-known experimental results in the context of sum harmonic generation efficiency with a 99% accuracy. The presented mathematical formulations can be used to design microscale optical parametric amplifiers to be employed in integrated photonics, MEMS devices, and optical communications.

REFERENCES

1. Chung, I., J.-H. Song, J. I. Jang, A. J. Freeman, and M. G. Kanatzidis, "$Na_2Ge_2Se_5$: A highly nonlinear optical material," *Journal of Solid State Chemistry*, November 2012.
2. Rout, A., G. S. Boltaev, R. A. Ganeev, Y. Fu, S. K. Maurya, V. V. Kim, K. S. Rao, and C. Guo, "Nonlinear optical studies of gold nanoparticle films," *Nanomaterials*, Vol. 9, 291, 2019.
3. Wu, R., J. Collins, L. T. Canham, and A. Kaplan, "The influence of quantum confinement on third-order nonlinearities in porous silicon thin films," *Appl. Sci.*, Vol. 8, 1810, 2018.
4. Sakhno, O., P. Yezhov, V. Hryn, V. Rudenko, and T. Smirnova, "Optical and nonlinear properties of photonic polymer nanocomposites and holographic gratings modified with noble metal nanoparticles," *Polymers*, Vol. 12, 480, 2020.
5. Varin, C., R. Emms, G. Bart, T. Fennel, and T. Brabec, "Explicit formulation of second and third order optical nonlinearity in the FDTD framework," *Computer Physics Communications*, Vol. 222, January 2018.
6. Zygiridis, T. T. and N. V. Kantartzis, "Finite-difference modeling of nonlinear phenomena in time-domain electromagnetics: A review," *Applications of Nonlinear Analysis. Springer Optimization and Its Applications*, Vol. 134, Rassias T. (eds), Springer, Cham., 2018.
7. Xu, L., M. Rahmani, D. Smirnova, K. ZangenehKamali, G. Zhang, D. Neshev, and A. E. Miroshnichenko, "Highly-efficient longitudinal second-harmonic generation from doubly-resonant AlGaAs nanoantennas," *Photonics*, Vol. 5, 29, 2018.
8. De Ceglia, D., L. Carletti, M. A. Vincenti, C. De Angelis, and M. Scalora, "Second-harmonic generation in Mie-resonant GaAs nanowires," *Appl. Sci.*, Vol. 9, 3381, 2019.
9. Rocco, D., M. A. Vincenti, and C. De Angelis, "Boosting second harmonic radiation from AlGaAs nanoantennas with epsilon-near-zero materials," *Appl. Sci.*, Vol. 8, 2212, 2018.
10. Nguyen, D. T. T. and N. D. Lai, "Deterministic insertion of KTP nanoparticles into polymeric structures for efficient second-harmonic generation," *Crystals*, Vol. 9, 365, 2019.
11. Huang, Z., H. Lu, H. Xiong, Y. Li, H. Chen, W. Qiu, H. Guan, J. Dong, W. Zhu, J. Yu, Y. Luo, J. Zhang, and Z. Chen, "Fano resonance on nanostructured lithium niobate for highly efficient and tunable second harmonic generation," *Nanomaterials*, Vol. 9, 69, 2019.
12. Cheng, T., Y. Xiao, S. Li, X. Yan, X. Zhang, T. Suzuki, and Y. Ohishi, "Highly efficient second-harmonic generation in a tellurite optical fiber," *Optics Letters*, Vol. 44, No. 19, 2019.
13. Kumar, S. and M. Sen, "High-gain, low-threshold and small-footprint optical parametric amplifier for photonic integrated circuits," *J. Opt. Soc. Am. B*, Vol. 35, 362–371, 2018.
14. *APL Photonics*, Vol. 4, 086102, 2019, https://doi.org/10.1063/1.5103272.
15. Milton, M. J. T., T. J. McIlveen, D. C. Hanna, and P. T. Woods, "A high-gain optical parametric amplifier tunable between 3.27 and 3.65 μm," *Optics Communications*, Vol. 93, Nos. 3–4, 186–190, 1992, ISSN 0030-4018, https://doi.org/10.1016/0030-4018(92)90526-W.
16. Wnuk, P., Y. Stepanenko, and C. Radzewicz, "High gain broadband amplification of ultraviolet pulses in optical parametric chirped pulse amplifier," *Optics Express*, Vol. 18, No. 8, 7911–7916, Apr. 2010.
17. Ooi, K., D. Ng, T. Wang, et al., "Pushing the limits of CMOS optical parametric amplifiers with USRN: Si_7N_3 above the two-photon absorption edge," *Nat. Commun.*, Vol. 8, 13878, 2017, https://doi.org/10.1038/ncomms13878.
18. Wei, X., Y. Peng, X. Luo, T. Zhou, J. Peng, Z. Nie, and J. Gao, "High-efficiency mid-infrared optical parametric amplifier with approximate uniform rectangular pump distribution," *Proc. SPIE 10436, High-Power Lasers: Technology and Systems, Platforms, and Effects*, 104360I, Oct. 26, 2017, https://doi.org/10.1117/12.2276963.
19. Aşırım, Ö. E. and M. Kuzuoğlu, "Super-gain optical parametric amplification in dielectric micro-resonators via BFGS algorithm-based non-linear programming," *Appl. Sci.*, Vol. 10, 1770, 2020.
20. Aşırım, Ö. E. and M. Kuzuoglu, "Enhancement of optical parametric amplification in micro-resonators via gain medium parameter selection and mean cavity wall reflectivity

adjustment," *Journal of Physics B: Atomic, Molecular and Optical Physics*, Apr. 2020, https://doi.org/10.1088/1361-6455/ab8947.

21. Coetzee, R. S., A. Zukauskas, J. M. Melkonian, and V. Pasiskevicius, "An efficient 2 µm optical parametric amplifier based on large-aperture periodically poled RB:KTP," *Proc. SPIE 10562, International Conference on Space Optics — ICSO 2016*, 105620L (25 September 2017), https://doi.org/10.1117/12.2296082.
22. Liu, X., R. Osgood, Y. Vlasov, et al., "Mid-infrared optical parametric amplifier using silicon nanophotonic waveguides," *Nature Photon*, Vol. 4, 557–560, 2010, https://doi.org/10.1038/nphoton.2010.119.
23. Gonzalez, M. and Y. Lee, "A study on parametric amplification in a piezoelectric MEMS device," *Micromachines (Basel)*, Vol. 10, No. 1, 19, 2018.
24. Al-Mahmoud, M., A. A. Rangelov, V. Coda, and G. Montemezzani, "Segmented composite optical parametric amplification," *Appl. Sci.*, Vol. 10, 1220, 2020.
25. Kida, Y. and T. Imasaka, "Four-wave optical parametric amplification in a raman-active gas," *Photonics*, Vol. 2, 933–945, 2015.
26. Manzoni, C. and G. Cerullo, *J. Opt.*, Vol. 18, 103501, 2016.
27. Wang, K.-Y. and A. C. Foster, *J. Opt.*, Vol. 17, 094012, 2015.
28. Schmidt, B., N. Thiré, M. Boivin, et al., "Frequency domain optical parametric amplification," *Nat. Commun.*, Vol. 5, 3643, 2014, https://doi.org/10.1038/ncomms4643.
29. Dao, L., K. Dinh, and P. Hannaford, "Perturbative optical parametric amplification in the extreme ultraviolet," *Nat. Commun.*, Vol. 6, 7175, 2015, https://doi.org/10.1038/ncomms8175.
30. Ilday, F. Ö. and F. X. Kärtner, "Cavity-enhanced optical parametric chirped-pulse amplification," *Opt. Lett.*, Vol. 31, 637–639, 2006.
31. Aşırım, Ö. E. and M. Kuzuoğlu, "Optimization of optical parametric amplification efficiency in a microresonator under ultrashort pump wave excitation," *International Journal of Electromagnetics and Applications*, Vol. 9, No. 1, 14–34, 2019.
32. Yang, M., et al., "An octave-spanning optical parametric amplifier based on a low-dispersion silicon-rich nitride waveguide," *IEEE Journal of Selected Topics in Quantum Electronics*, Vol. 24, No. 6, 1–7, Art No. 8300607, Nov.–Dec. 2018.
33. Varin, C., G. Bart, T. Fennel, and T. Brabec, "Nonlinear Lorentz model for the description of nonlinear optical dispersion in nanophotonics simulations [Invited]," *Opt. Mater. Express*, Vol. 9, 771–778, 2019.
34. Boyd, R. W., *Nonlinear Optics*, 105–107, Academic Press, New York, 2008.
35. Saleh, B. E. A. and M. C. Teich, *Fundamentals of Photonics*, 885–917, Wiley-Interscience, New York, 2007.
36. Nocedal, J. and S. J. Wright, *Numerical Optimization*, 36–37, Springer, New York, 2006.
37. Aşırım, Ö. E., "Super-gain parametric wave amplification in optical micro-resonators using ultrashort pump waves," Middle East Technical University Library, 2020.
38. Paschotta, R., "Article on 'optical parametric amplifiers'," *Encyclopedia of Laser Physics and Technology*, 1st Edition, Wiley-VCH, Oct. 2008, ISBN 978-3-527-40828-3.
39. Yang, Y., D. Zhu, W. Yan, et al., "A general theoretical and experimental framework for nanoscale electromagnetism," *Nature*, Vol. 576, 248–252, 2019.
40. Abubakar, A. B., P. Kumam, H. Mohammad, A. M. Awwal, and K. Sitthithakerngkiet, "A modified Fletcher-Reeves conjugate gradient method for monotone nonlinear equations with some applications," *Mathematics*, Vol. 7, 745, 2019.
41. Sellami, B. and M. C. E. Sellami, "Global convergence of a modified Fletcher-Reeves conjugate gradient method with Wolfe line search," *Asian-European Journal of Mathematics*, Vol. 13, No. 04, Jun. 2020.
42. Pang, D., S. Du, and J. Ju, "The smoothing Fletcher-Reeves conjugate gradient method for solving finite minimax problems," *Science Asia*, Vol. 42, 40–45, 2016.

43. Frazer, L., J. K. Gallaher, and T. W. Schmidt, "Optimizing the efficiency of solar photon upconversion," *ACS Energy Letters*, Vol. 2, No. 6, 1346–1354, 2017.
44. Seo, Y.-K., J.-H. Seo, and W.-Y. Choi, "Photonic frequency-upconversion efficiencies in semiconductor optical amplifiers," *Photonics Technology Letters*, Vol. 15, 751–753, IEEE, 2003.
45. Tan, W., X. Qiu, G. Zhao, et al., "High-efficiency frequency upconversion of 1.5 μm laser based on a doubly resonant external ring cavity with a low finesse for signal field," *Appl. Phys. B*, Vo. 123, 52, 2017, https://doi.org/10.1007/s00340-016-6626-2.